Background Modeling For Target Detection And Recognition

Bir Bhanu and **Songnian Rong**
College of Engineering
University of California
Riverside, California 92521

Abstract

In order to reduce false alarms and to improve the detection and recognition performance in cluttered environments, it is important to develop not only the models for man-made targets but also the models of natural backgrounds. In this paper, we present a learning based approach to construct and to maintain a concise and accurate background model bank by *learning from positive and negative examples.* Features used to characterize the natural backgrounds include joint space-frequency features based on the Gabor transform, and localized statistics of geometric elements. An open-structure representation is used to manage the background modeling process so that it is easy to include new sensors, new features and other contextual information. Initial results are presented using visible and infrared (IR) images.

1 Introduction

Automatic Target Detection and Recognition (ATD/R) is a challenging application for the general techniques developed by image processing and image understanding communities. There are several reasons that contribute to this challenge: (a) a target may appear in many different backgrounds and it tends to be mixed up with its surroundings, (b) signatures of a target strongly depends upon the background surrounding the target and environmental conditions, and (c) signatures of a target are generally not repeatable. As a result, early stage target-signature-based image segmentation is generally unreliable. Since the ATR process is a serial process, any target we fail to detect during the detection stage will be lost forever. In the detection stage, we would like to single out every suspicious target area, even at the cost that we may bring in some false target areas by doing so. Then it is the responsibility of the following recognition stage to verify the identity of each real target and to filter out the false targets. An ideal ATR system is the one that (1) does not miss any potential target area in the detection stage, and (2) does not verify any non-target area in the recognition stage.

To achieve the goal of high detection probability and simultaneous low false-alarm rate, we present a new strategy called Background Model Aided Target Detection and Recognition (BMATDR) [10]. The main idea of BMATDR is to use explicit background models, as well as target models, throughout the ATR process (Figure 1). During the detection stage, any area (region-of-interest) that is selected by the target models or that is not selected by the background models is labeled as a potential target area and is passed to two parallel recognition processes. In the target recognition process, each candidate area is verified against target models and the verified identity along with the corresponding confidence value C_{tgt} is attached to the area. The background recognition process is the same except that the models used are background models (the corresponding confidence value is noted as C_{bgd}). The results from the above recognition stage (areas with identity labels and confidence values) are passed to the third stage for cross-validation, where we finally label areas that have consistent answers from the two recognition

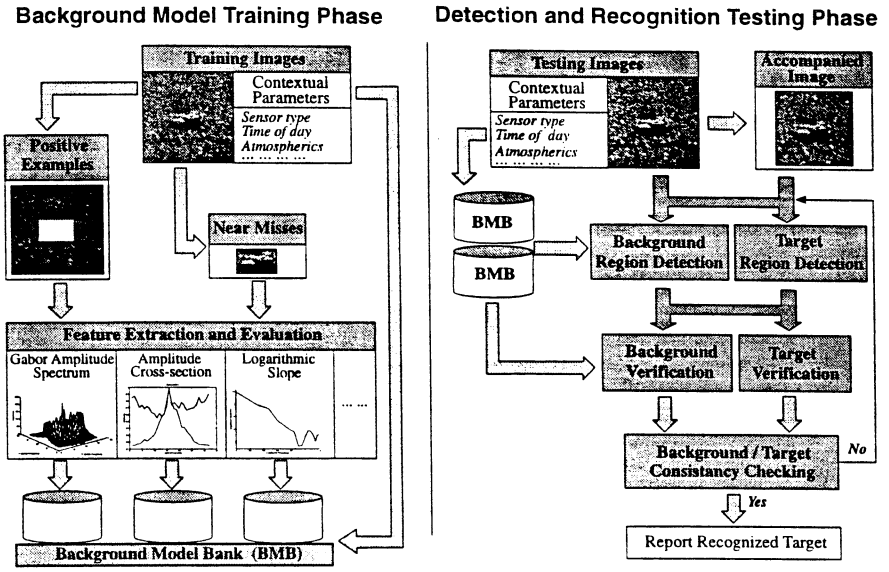

Figure 1: Background model-aided target detection and recognition system. To get the best discriminating result, feature cell size is selected as the size of a potential target, which, in turn, is determined using the range information given as a contextual parameter. The accompanied image is constructed from the testing image by removing rows and columns, equal to one half the size of the selected feature cell, from all the four sides.

processes and resolve any conflicts. Areas with a high C_{tgt} and a low C_{bgd} are labeled as target areas while areas with a low C_{tgt} and a high C_{bgd} are labeled as background areas. A low C_{tgt} with a low C_{bgd} may indicate a non-target object, while a high C_{tgt} and a high C_{bgd} point out the cases that have to be resolved based on the characteristics of the application.

In the following section, we discuss our approach based on supervised self-organizing maps to construct models for natural backgrounds. In Section 3, we examine the feature groups that we have developed for characterizing natural backgrounds. Experimental results are shown in Section 4. Section 5 concludes this paper with a summary of the completed work and future research directions.

2 General Approach

In recent years, two distinct approaches have been developed by ATR researchers to characterize the natural background (or thermal clutters) in infrared images. In the *first* approach, heat transfer equations are used to model the thermal behaviors of different materials. [4, 5, 14]. Although theoretical models have been enhanced with more accurate mathematical description of the physics involved in the heat exchange process, they still have a long way to go before these models can be effectively used in practical applications. The main reason is that there are too many environmental factors that can affect the thermal behavior of the target and the background. Sherman et al. [7] categorized 41 such variables into five classes — background parameters, target parameters, platform dynamics, atmospherics and sensor parameters. The *second* approach focuses on the image features rather than the thermal-physical meaning behind these images. Researchers following the second approach mainly address two different tasks: (a) quantify the clutter in infrared images and use the clutter measure to understand how the clutter affects the detection performance in a target detection system with man-in-the-loop [9, 13]. (b) build statistical models for different natural backgrounds, and use these models in an ATR system [6]. Our BMATDR approach (Figure 1) was

developed to accomplish the second task.

Since the new, improved sensors have increased the resolution of IR images, it is now possible to extract, from these images, many useful image features that can be used to characterize the background. Two important goals of our image feature-based background modeling approach presented in this paper are:

- to develop features that can effectively characterize a certain natural background against man-made target(s) and other backgrounds.
- to develop a suitable representation for the background model so that we can control the potential risk of memory explosion while learning the background models from real images.

Since a natural background makes sense to human eyes only when a sufficient area of that background has been seen, region-based features are more suitable for characterizing a natural background than global or pixel based features. To facilitate the following discussion, we introduce two terms, **feature cell** and **feature cell size**, which will be used throughout this paper to refer regions used in feature computation.

Definition: *A Feature Cell is a rectangular region within the image from which an image feature is computed. The Feature Cell Size is a measure of this rectangular region.*

2.1 The Background Model Bank

Since natural backgrounds can occur in a wide variety, background characterization must rely on multiple features. To efficiently use the available features, we need a proper representation to hold the information efficiently. One approach to attack such a problem is to organize all the features into a high dimensional feature vector (i.e. long feature vector) and classify a background based on the position of the corresponding feature vector in some high-dimensional feature space [6]. The other approach is based on short feature vectors. The key idea behind this later scheme is the need to understand the physical meaning of each feature and put each feature in a group of features that have closely related physical meanings. In our work, we follow the second approach and restrict the size of each group so that the size of any feature group is not more than three. If new feature metrics are found to be useful for background modeling, we would construct a new feature group rather than increasing the size of an existing group. We investigate the discriminating power of each feature group separately, and build a background model for each such group. Thus, for a given background we will have a collection of simple (i.e. low-dimensional) models. We refer to such a collection of models as a *Background Model Bank (BMB)*, and each model in this bank as a *BMB member*. Each BMB member characterizes a given background from a specific physical view point. Figure 2 shows how this BMB would work once it has been constructed. The *validity scope* of a BMB member is a lookup table, indexed by *contextual parameters*, which stores the performance of a BMB member under certain conditions. Major contextual parameters include sensor types, range, depression angle, weather conditions, etc. A *reinforcement learning* algorithm is now under development to facilitate the determination of validity scopes.

2.2 Representation of a BMB member using a self-organizing feature map

Although many papers in the literature have used known statistical distributions in their analysis of natural clutters in IR images, there is no strong evidence that thermal natural clutters possess a certain statistical distribution [9]. Instead of artificially assigning a distribution model to background models, we construct our BMB from real images through a supervised learning process. Since reliable statistical models can only be obtained through analysis of a large population of samples, space and time complexities of algorithms become a major concern when selecting a learning scheme. In our approach, each BMB member is represented by a self-organizing map (SOM). By controlling the size of the SOM, we can easily control the space and time complexity of the learning process. Figure 3 shows

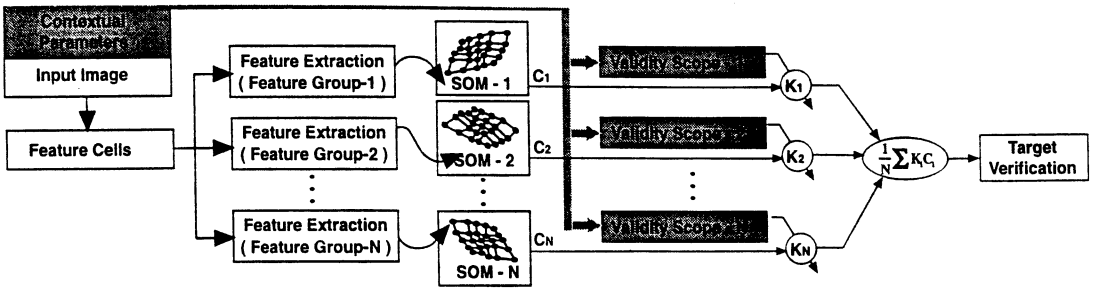

Figure 2: Using the learned Background Model Bank (BMB) for target detection. The *validity scope* of a BMB member is a lookup table, indexed by *contextual parameters*, which stores the performance of a BMB member under certain conditions. C_i's are confidences for background classification using different feature groups. K_i's are weights of different feature groups under given environmental conditions. They are learned by using reinforcement learning.

the training process for a BMB member. A supervised SOM algorithm has been developed to accomplish learning for BMB members from training examples [11].

3 Feature Groups

3.1 Gabor transform-based features

Features in the frequency domain have been widely used for accomplishing tasks like *texture segmentation* [1]. A special difficulty associated with ATR applications is that in most situations, a target of interest constitutes only a small part of the sensed image. Therefore, if a feature is based on global transforms like the Fourier transform, it is very likely that the existence of the target may not affect the spectrum to an extent that it is clearly discernible. But if the spectrum can be localized to an area whose size is comparable to the size of a target, the spectrum would have a recognizable variation (with respect to background) when the "attention window" is placed on top of the target. One approach to achieve this localized spectra is by using the Gabor transform. Gabor transform can be considered as a special case of short range Fourier transform. It is different from the Fourier transform in the sense that it can decompose an input image into basis functions which are localized both in spatial and frequency domain. This property is particularly desirable for ATR application. To compute the discrete Gabor transform of an image, we implemented an algorithm which makes the otherwise complex computation more efficient [15].

The 2-D Gabor Elementary Functions (GEF) are defined as

$$g_{mnrs}(x,y) = g(x - mM, y - nM) \cdot \exp\left[2\pi i \left\{\frac{h(r)h(x)}{M} + \frac{h(s)h(y)}{M}\right\}\right], \text{ where } h(t) = t - \tfrac{M-1}{2}, \tag{1}$$

and M is the feature cell size which determines the spatial resolution of the transform. A larger M corresponds to a coarser spatial resolution and finer frequency resolution, while a smaller M corresponds to a finer spatial resolution and coarser frequency resolution. Function $g(u,v)$ is the window function that localizes the GEF in spatial domain. For a 2-D square image $Im(x,y)$, $x = 0, 1, \cdots, KM-1$, and $y = 0, 1, \cdots, KM-1$, the 2-D discrete Gabor transform can be expressed as

$$Im(x,y) = \sum_{m=0}^{K-1}\sum_{n=0}^{K-1}\sum_{r=0}^{M-1}\sum_{s=0}^{M-1} a_{mnrs}\, g_{mnrs}(x,y) \tag{2}$$

where a_{mnrs} is the Gabor coefficient corresponding to GEF $g_{mnrs}(x,y)$. If $g_{mnrs}(x,y)$ is separable, which is the case when we use 2-D Gaussian function as the window function, the Gabor decomposition can be written in matrix form

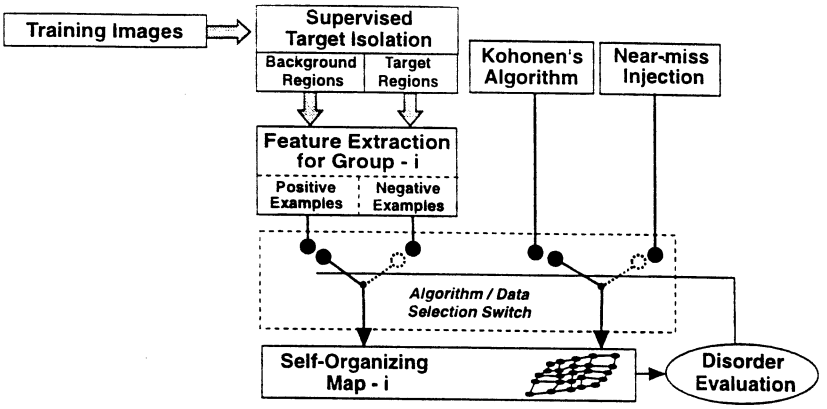

Figure 3: Building up a member of the Background Model Bank. The initial uniformly distributed self-organizing map (SOM) is trained first by using positive examples and Kohonen's algorithm. After a pre-selected number of iterations, a disorder index is computed. If the map has reached a certain degree of ordering, the algorithm/data selection switch is turned to the near-miss injection algorithm which uses negative examples to refine the trained SOM. To allow a BMB member to memorize its valuable past knowledges while it gains new experiences, the size of the SOM needs to be extensible. An incremental SOM algorithm allows us to achieve this.

as $Im = GAG^T$, where Im is the $KM \times KM$ image matrix, and A is the $KM \times KM$ Gabor coefficient matrix. Matrix G and its transpose can be pre-calculated based on the selected spatial resolution. To compute the transform, we have

$$A = G^{-1} Im (G^T)^{-1} \tag{3}$$

Each element of matrix A is complex and represented by its real part ar_{rs}^{mn} and imaginary part ai_{rs}^{mn}. Here m and n are the two spatial indexes that locate the element in spatial domain, while r and s are the two frequency indexes that locate the element in frequency domain. The amplitude of the transform is given by

$$Am_{rs}^{mn} = \left((ar_{rs}^{mn})^2 + (ai_{rs}^{mn})^2 \right)^{1/2} \tag{4}$$

Three feature groups are constructed from the Gabor amplitude spectrum.

3.1.1 Group 1: Multi-level mean amplitudes of Gabor transform

The *first* group consists of three features — $MA0$, $MA1$ and $MA2$, which are the zero, first, and second level mean amplitudes of a feature cell. To compute them, the discrete Gabor amplitudes are first sorted in a decreasing order. If $\hat{Am}(i)$ denotes the sorted Gabor amplitudes of a $M \times M$ feature cell, $i = 0, 1, \cdots, M^2 - 1$, then

$$MA0 = \frac{1}{M^2} \sum_{i=0}^{M^2-1} \hat{Am}(i), \qquad MA1 = \frac{2}{M^2} \sum_{i=0}^{(M^2-1)/2} \hat{Am}(i), \qquad MA2 = \frac{4}{M^2} \sum_{i=0}^{(M^2-1)/4} \hat{Am}(i) \tag{5}$$

3.1.2 Group 2: Moments of the Gabor amplitude spectrum

The *second* group consists of two features — the first order moments of the Gabor amplitude spectrum with respect to ω_x and ω_y axis.

$$Mom_x = \sum_{r=1}^{M-1} \sum_{s=0}^{M-1} Am(r,s) \cdot r, \qquad Mom_y = \sum_{r=0}^{M-1} \sum_{s=1}^{M-1} Am(r,s) \cdot s \tag{6}$$

3.1.3 Self-similarity phenomenon in natural scenes

It has been recognized that images of natural scenes exhibit statistical self-similarity at different scales [8]. Such a property of self-similarity, also called fractal phenomenon, has been used by computer vision researchers for understanding the images of natural scenes, e.g. image segmentation based on fractal features [12]. In addition to the *fractal dimension*, which is the most popular fractal feature used in the literature, other statistical features can also be used to describe the fractal phenomenon within images. Field [2, 3] has proposed a feature which relates the fractal phenomenon occuring in an image with the amplitude spectrum of the image. Assume we have an image whose energy density at spatial frequency k is $g(k)$. Then the total energy at this frequency would be $E(k) = (2\pi k)g(k)$. The energy within a frequency band between frequency k and nk is

$$E_k^{nk} = \int_k^{nk} E(k)dk = \int_k^{nk} (2\pi k)g(k)dk \tag{7}$$

Scaling the image by a factor of a will bring this amount of energy to a new frequency band which goes from frequency ak to frequency ank. If the image exhibits fractal phenomenon, this scaling process should not affect the energy we just computed. Since this is true for any a and k, the only possibility is

$$E_k^{nk} = \int_k^{nk} (2\pi k)g(k)dk = Constant \tag{8}$$

which requires

$$g(k) \propto 1/k^2 \tag{9}$$

Equation 9 shows that the energy spectrum falls off as $1/k^2$. Therefore, the amplitude spectrum will fall of as $1/k$. If we plot the logarithmic amplitude vs. logarithmic frequency, the plot will be a straight line with a slope of -1. Field [3] showed that the mean slope, for 85 visible images of different natural scenes, was -1.1.

Since one of the major functions of our background model is to discriminate natural backgrounds from man-made objects, this feature can be very useful if images of the man-made objects do not show this -1 slope. Again, since targets may constitute only a small part of the image, we use Gabor transform, rather than Fourier transform (as Field did in [2]), as the basis for computing this feature. To compute the slope feature, we first need to compute the average Gabor amplitude at each frequency over all the available orientations. Since the amplitude spectrum obtained from Equation 2 is a square matrix, interpolation is needed to find out the correct amplitudes along all the orientations except orientation 0^o and 90^o. To make the computation easier, we consider only 8 orientations at each frequency, namely $0^o, 45^o, 90^o, 135^o, 180^o, 225^o, 270^o$, and 315^o. Let $\bar{Am}_k$ denote the average Gabor amplitude at spatial frequency f_k $(k = 1, 2, \cdots, M-1)$, a least-square method is used to fit a straight line to the data pairs of $(\log \bar{Am}_k, \log f_k)$. The slope of the fitted line and the maximum error of this linearization are computed as features according to

Group 3:

$$SLP = \frac{\sum_{k=1}^{M-1} f_k \sum_{k=1}^{M-1} \bar{Am}_k - (M-1)\sum_{k=1}^{M-1} f_k \bar{Am}_k}{\left(\sum_{k=1}^{M-1} f_k\right)^2 - (M-1)\sum_{k=1}^{M-1} {f_k}^2} \tag{10}$$

$$ERR = \left\{ \max_{k=1}^{M-1} (SLP f_k + B - \bar{Am}_k) - \min_{k=1}^{M-1} (SLP f_k + B - \bar{Am}_k) \right\} \cos(\arctan(SLP)) \tag{11}$$

where

$$B = \frac{1}{M-1}\left(\sum_{k=1}^{M-1} \bar{Am}_k - SLP \sum_{k=1}^{M-1} f_k\right) \tag{12}$$

Another feature that we have found useful in distinguishing different natural backgrounds in visible images is the difference between the two cross-section curves of the Gabor amplitude spectrum along orientation 0^o and 90^o.

3.2 Group 4: Local statistics of geometric elements

The number of edges in a neighborhood has been used as a feature for texture classification in visible images. Since many natural backgrounds show a certain degree of texture, similar features that measure the local statistics of geometric elements can be used for natural background characterization. In FLIR images, a target normally appears as one or several blobs close to each other, but, due to the varying contrast, the target-background border is not always distinct. So, in addition to measuring the local number of edges, we use the number of blobs and the average size of blobs in a feature cell as features. To find out the blobs in a selected feature cell, we run a blob-coloring algorithm over the image with different thresholds. After each blob-coloring, statistics of the size, shape, and population of the blobs in a feature cell are computed as features. We have found in our experiments that the change of these local statistics with respect to different thresholding values reveals some characteristics of natural backgrounds. In this paper, we are focusing on the number of the blobs vs. the gray value threshold. When we plot these two variables on a semi-logarithmic plot, it can be seen that the lines corresponding to the target regions exhibit smaller slope than the lines corresponding to the background regions (Figure 7). We can compute the slope of these lines as a feature using

$$S_{blb} = \frac{\sum_{k=1}^{N} k \sum_{k=1}^{N} \log\left(N_{blb}(k)\right) - N \sum_{k=1}^{N} k \log\left(N_{blb}(k)\right)}{\left(\sum_{k=1}^{N} k\right)^2 - N \sum_{k=1}^{N} k^2} \tag{13}$$

where N is the highest threshold used, and $N_{blb}(k)$ denotes the number of blobs in a feature cell when we use threshold k.

Algorithm Adaptive-Region-Growing(Im, Th)
Im : input image.
Th : region growing threshold.
begin
for (each pixel in Im, from left to right, top to bottom) **do**
Let p_c = gray value of the current pixel **C**.
Let p_u = gray value of the upper pixel **U**.
Let p_l = gray value of the left pixel **L**.
if (**abs**$(p_c - p_u) \leq Th$ && **abs**$(p_c - p_l) > Th$) **then**
Include **C** into the blob that contains **U**.
Update the average gray value, B_{val}, of the blob.
Update the gray value of each pixel in the blob to B_{val}.
else if (**abs**$(p_c - p_l) \leq Th$ && **abs**$(p_c - p_u) > Th$) **then**
Include **C** into the blob that contains **L**.
Update the average gray value, B_{val}, of the blob.
Update the gray value of each pixel in the blob to B_{val}.
else if (**abs**$(p_c - p_l) > Th$ && **abs**$(p_c - p_u) > Th$) **then**
Create a new blob.
Include **C** into this blob.
$B_{val} = p_c$.
else if (**abs**$(p_c - p_l) \leq Th$ && **abs**$(p_c - p_u) \leq Th$) **then**
if (**abs**$(p_c - p_u) \leq$ **abs**$(p_c - p_l)$) **then**
Include **C** into the blob that contains **U**.
else
Include **C** into the blob that contains **L**.
end if
Update the average gray value, B_{val}, of the blob.
Update the gray value of each pixel in the blob to B_{val}.

if (**abs**($p_u - p_l$) $\leq Th$) **then**
Merge the blob that contains **L** to the blob that contains **U**.
Update the gray value, B_{val}, of the merged blob.
Update the gray value of each pixel in the merged blob to B_{val}.
end if
endif
end for
end Algorithm

---

4 Experimental Results

In this section, we show experimental results of using Gabor transform-based features and local statistics of geometric elements to characterize natural backgrounds. Samples of FLIR and low resolution visible images used in our experiments are shown in Figure 4, where a man-made target is present on top of a natural terrain. All the images are of size 200 × 200. To build up the background models, we manually "cut out" the pure background regions from these training images and use them as positive training examples. Figure 7, 5, and 6 show the values of different feature groups computed from the sample images using a 50 × 50 feature cell size.

All the features show a certain degree of discriminating power between man-made targets and natural backgrounds. However, we have found that the separation of these two classes (background and man-made target) becomes less than 100% when examples exhibiting different contextual parameters are used. This degradation in the discriminating power calls for the cooperation of multiple feature groups and a measure to resolve the feature overlapping problem in each feature group. Our work is continuing to complete the system as shown in Figure 1 and 2. At this time we have completed the feature extraction and the building up of BMB members via supervised SOM learning in Figure 2.

5 Conclusions

In this paper, we presented an approach that uses self-organizing maps to construct statistical models of natural backgrounds using visible and infrared images. By alternately using positive examples and near-misses in the training phase, the SOM can learn the distribution of feature vectors and refine its boundaries to deal with the feature

(a) (b) (c)

Figure 4: Sample images used in our experiments, (a),(b): FLIR images, (c): low-resolution visible image.

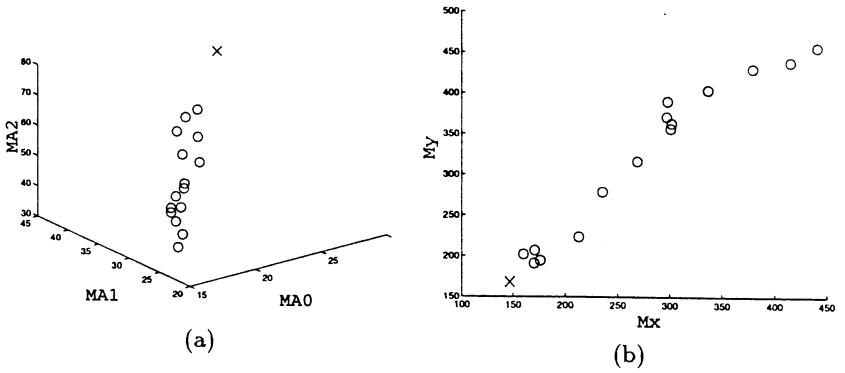

(a) (b)

Figure 5: Gabor amplitude spectrum features: (a) multilevel mean magnitude of Gabor amplitude computed from the image shown in Figure 4(a). (b) first order moments of the Gabor amplitude spectrum computed from the image shown in Figure 4(c), (o : background, x : target).

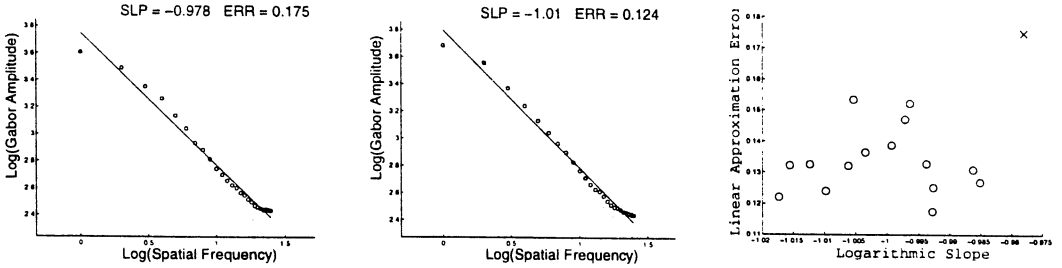

(a) (b) (c)

Figure 6: Feature: slope of $\log(amplitude)$ vs. $\log(frequency)$ computed from the low resolution visible image shown in Figure 4(c). (a) target region. (b) background region. (c) distribution of the feature values, (o : background, x : target).

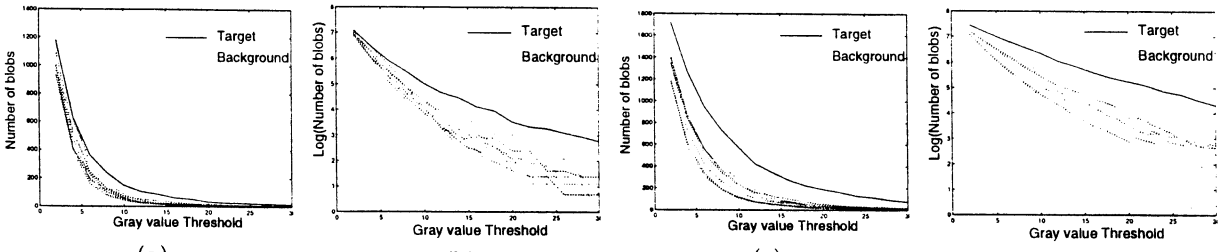

(a) (b) (c) (d)

Figure 7: Feature: local statistics of geometric elements. (a) number of blobs vs. gray value threshold for Figure 4(a). (b) logarithmic number of blobs vs. gray value threshold for Figure 4(a). (c) number of blobs vs. gray value threshold for Figure 4(b). (d) logarithmic number of blobs vs. gray value threshold for Figure 4(b).

overlapping problem. How beneficial the background models can be to ATD/R process depends on two factors, (1) the effectiveness of the selected features, and (2) better understanding of each feature's validity scope with respect to contextual parameters. Future work will concentrate on: (1) testing our approach on a large database of infrared and visible images, (2) identifying the most important contextual parameters for each feature group using reinforcement learning methods, and (3) extending our approach to other sensors including synthetic aperture radar.

6 Acknowledgments

This work was supported by ARPA grant MDA972-93-1-0010. The contents of the information do not necessarily reflect the position or the policy of the U.S. Government.

References

[1] F. D'Astous and M.E. Jernigan. Texture discrimination based on detailed measures of the power spectrum. In *Proceedings of the Seventh International Conference on Pattern Recognition*, pages 83–86, 1984.

[2] D.J. Field. Relations between the statistics of natural images and the response properties of cortical cells. *Journal of Optical Society of America*, 4(12):2379–2394, 1987.

[3] D.J. Field. Scale-invariance and self-similar 'wavelet' transforms: an analysis of natural scenes and mammalian visual systems. In J.C.R. Hunt M. Farge and J.C. Vassilicos, editors, *Wavelets, Fractals, and Fourier Transforms*, pages 151–194, Oxford, 1993. Clarendon Press.

[4] G. Howard. Thermal background modeling. *Proceedings SPIE*, 933:132–140, 1988.

[5] P. Jacobs. Review of the technology and research in the area of infrared signatures of targets and backgrounds. *Proceedings SPIE*, 1311:80–94, 1990.

[6] M.A. Noah, P.V. Noah, J. Schroeder, B.V. Kessler, and J. Chernick. Background characterization techniques for pattern recognition applications. *Proceedings SPIE*, 1098:55–70, 1989.

[7] J.W. Sherman, D.N. Spector, C.W. "Ron" Swonger, L.G. Clark, E.G. Zelnio, M.J. Lahart, and T.L. Jones. Automatic target recognition systems. In L. Shumaker, editor, *The Infrared and Electro-optical Systems Handbook*, pages 343–402. SPIE Optical Engineering Press, 1993.

[8] B.B. Mondelbrot. *The Fractal Geometry of Nature*. Freeman, 1983.

[9] W.R. Reynolds. Toward quantifying infrared clutter. *Proceedings SPIE*, 1311:232–240, 1990.

[10] B. Bhanu, R.N. Braithwaite, W. Burger, S. Das, S. Rong, and X. Wu. *Gabor Waveletets for Automatic Target Detection and Recognition, quarterly report to ARPA*. College of Engineering, University of California, Riverside, December, 1993.

[11] S. Rong and B. Bhanu. Characterizing natural backgrounds for target detection. In *Proc. ARPA Image Understanding Workshop*, Monterey, California, November 14-16 1994.

[12] B.B. Chaudhuri, N. Sarkar and P. Kundu. Improved fractal geometry based texture segmentation technique. *IEE Proceedings E (Computers and Digital Techniques)*, 140(5):233–241, 1993.

[13] S.R. Rotman, G. Tidhar and M.L. Kowalczyk. Clutter metrics for target detection system. *IEEE Trans. Aerospace and Electronic Systems*, 30(1):81–91, 1994.

[14] F.G. Wollenweber. Weather impact on background temperatures as predicted by an IR-background model. *Proceedings SPIE*. 1311:119–128, 1990.

[15] J. Yao. Complete Gabor transformation for signal representation. *IEEE Trans. Image Processing*, 2(2):152–159, April 1993.

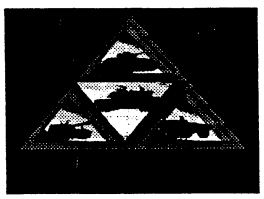

TARDEC

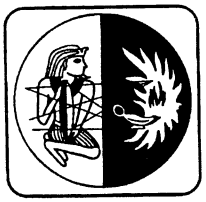

NVESD

KRC
Keweenaw Research Center

Volume I
Proceedings
Fifth Annual

Ground Target Modeling and Validation Conference

August 1994

at
Michigan Technological University
Houghton, Michigan